Heat Treat 2019: Proceedings of the
30th ASM Heat Treating Society Conference
October 15–17, 2019, Detroit, Michigan, USA

Microstructure Refinement Strategies in Carburized Steel

M. Agnani, O.L. DeNonno, K.O. Findley and S.W. Thompson
Metallurgical and Materials Engineering, Advanced Steel Processing and Products Research Center,
Colorado School of Mines, Golden, CO

Abstract

Microstructure refinement strategies in carburized microstructures were evaluated because of their potential for improving the fatigue performance of case carburized components. Commercial 52100 steel was used to simulate the high carbon content in the case. Specimens were subjected to various thermal treatments in a quenching dilatometer. Reheating cycles to austenitizing temperatures were evaluated with respect to both prior austenite grain size (PAGS) and associated martensite and retained austenite refinement. Quantitative stereological measurements were performed to evaluate the micro-geometry of plate martensite and the size distribution of retained-austenite regions. Decreasing the reheating temperature resulted in finer PAGS and multiple reheating cycles resulted in a narrow PAGS distribution. Refinement in PAGS led to a reduction in martensite plate size and finer distribution of RA.

Introduction

Carburized steel components find applications in vehicle powertrains, machines, and power-generation equipment where high strength is required in combination with good fatigue resistance [1]. These desirable properties can be attributed to complex microstructures consisting of plate martensite and retained austenite (RA) in the carbon-rich case and low-carbon microstructures in the core. There is a gradient of carbon concentration and hence RA content, microstructure, and hardness along the depth of the components [2]. Hence, it is imperative to advance our understanding of the characteristics of carburized microstructures for optimized processing and performance of drive-train components.

Wise and Matlock [3] performed a statistical analysis to correlate microstructural variables with bending fatigue endurance limits of carburized steels. Case grain size is the most critical parameter that influences endurance limits in carburized components [3]. Similarly, Apple and Krauss [4] showed that refinement of prior austenite grains in the case regions using reheating cycles led to improvements in fatigue performance. During reheating to elevated temperatures, austenite grains nucleate and grow on prior austenite grain boundaries (PAGBs) and at martensite/austenite interfaces. They subsequently impinge against one another resulting in fine austenitic grains and hence a fine quenched final microstructure. Krauss [2] reported that triple reheating treatments led to a three times reduction in prior austenite grain size (PAGS) of carburized 4320 steel throughout the carburized case.

The prior austenite grain size influences martensite transformation kinetics. The mechanism of growth of martensite from austenite is displacive and occurs at about the speed of sound in steel [5]. As a result, it is experimentally complicated to study, resolve and interpret the nucleation and growth events. Two common martensite morphologies are found in steels: lath and plate, where the latter is common in high-carbon microstructures. Three different modes of kinetics are predominantly discussed in the literature: athermal, isothermal, and burst kinetics [6]. Though there is extensive literature on isothermal and burst kinetics of martensite growth in Fe-Mn-Ni systems [7, 8], athermal martensite is usually observed in low-alloy carbon steel [5].

In steels, transformation of austenite to martensite proceeds upon lowering the temperature below the martensite start temperature, M_s and is not a function of time, hence the name athermal. The transformation extends to a temperature range between M_s and a certain temperature M_f below which no transformation takes place even in the case of the presence of untransformed austenite. Under isothermal conditions at a temperature between M_s and M_f, the transformation rate rapidly slows, but increases upon further lowering of temperature [6]. Stereological methods have been previously used to investigate and mathematically formalize the mechanisms and kinetics of martensite formation and to characterize the plate-martensite-and-RA microstructure [9–11].

Previous stereological studies suggest that PAGBs strongly influence nucleation of martensite. In early stages of transformation, Chang *et al.* [9] observed that in coarse grain microstructures a greater fraction of martensite plates nucleate at PAGBs than in fine-grained samples. However, in the later stages of transformation, no differences were observed for the autocatalytic tendencies (*i.e.,* nucleation of new plates on existing plates) of plates at PAGBs and plates within austenite grains [9]. PAGS also influences the so-called “spread” of martensite [11]. The spread of transformation kinetics is different for large and small grains. Large grains promote uniform spread and fill-in of martensite transformation whereas small grains show partially transformed clusters of grains and in the later stages of the transformation, plate formation gradually spreads in all austenitic grains [12].

PAGS influences both the martensite transformation and the endurance limits in carburized components. However, the link between martensitic microstructure and fatigue performance is not well established. In this investigation, stereological methods are employed to provide a quantitative basis for the evaluation of refinement in plate martensite and RA constituents associated with refinement of PAGS during thermal cycling.

Experimental Procedures

In this study, commercially available high-carbon 52100 steel bar was used as a simulation alloy for the case region of carburized components to promote plate morphology of martensite. The composition of the steel is given in Table 1. Trace amounts of Mo, Ti, Nb, Al, S, P and Cu were present. Cylindrical samples with a diameter of 4 mm and length of 10 mm were machined out of an 82.6-mm-diameter bar from the half-radius position. The specimens were used to perform controlled heat treatments using a TA Instruments Type 805L quenching dilatometer.

Table 1. Composition of 52100 Steel (in wt pct)

C	Mn	Si	Ni	Cr	Al	N	Fe
1.00	0.35	0.26	0.13	1.40	0.024	0.007	bal.

The as-received microstructure consisted of pro-eutectoid cementite along the PAGB and pearlite colonies (colony size - 68.9μm ± 3.9μm; A_{C1} = 780 °C; A_{CM} = 793 °C). All samples were heated to 1000 °C at 5°C/s (constant for all subsequent heat treatments), held isothermally for 100 s and quenched to room temperature at 10 °C/s to form a baseline martensitic microstructure similar to that present in the case of a carburized microstructure. In the subsequent thermal cycling step, samples were reheated to three different austenitizing temperatures, 900 °C, 1000 °C or 1100 °C, held isothermally for 100s and quenched to ensure martensitic formation. Further, to study the influence of time, a short reheating treatment was performed at 900 °C for 1s. Up to three short reheating cycles (designated as RHS – n where n is number of cycles) at 900 °C for 1s were also carried out to study the evolution of PAGS during thermal cycling. Fig. 1 shows the summary of thermal cycles.

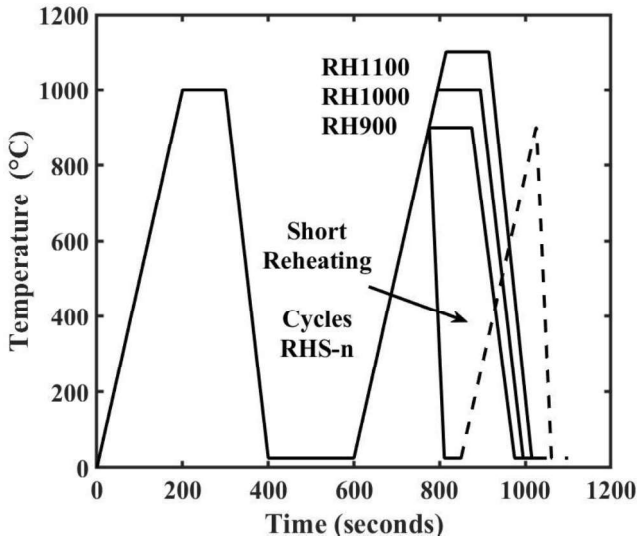

Figure 1: Schematic diagram showing thermal history during thermal cycling heat treatments.

Cross-sections of samples were hot mounted in bakelite at 140 °C and polished using standard metallographic procedures. Samples were etched with saturated picric acid to reveal the PAGBs and with 2 pct nital to quantify the martensite plates and RA sizes. Abrams three circle method was used to evaluate the PAGS of samples from picral etched light micrographs according to ASTM E112. Stereological measurement of the martensite micro-geometry was performed on scanning electron micrographs using standard stereological techniques such as point counting and lineal intercept counting [13]. Figure 2 schematically shows the evaluated stereological quantities: surface area per unit volume of martensite midplane (S_V^{MID}) and length per unit volume of midplane periphery (L_V^{MID}). Image processing was used to determine the size distribution of RA.

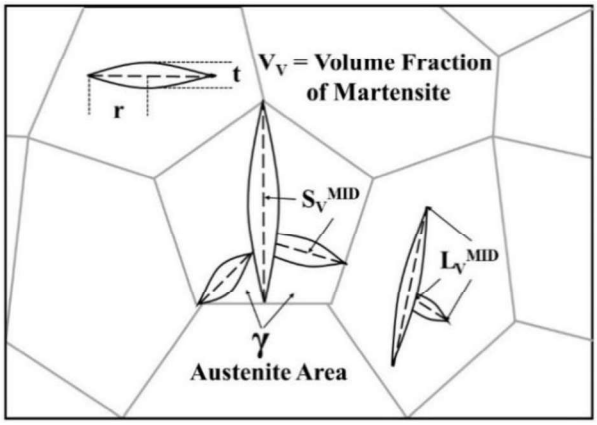

Figure 2: A schematic drawing showing various stereological quantities measured during the investigation.

Results and Discussion

Prior Austenite Grain Size

Figure 3 shows a light optical micrograph of a cross-section of RH1000 sample etched with saturated picric acid. The PAGBs are prominent; however due to over-etching, the martensite-RA substructure is visible in certain regions too. The RH1000 sample showed significant microstructural banding of grain sizes possibly due to alloy segregation and compositional banding during prior processing. The narrow bands consisting of significantly smaller PAGS were systematically avoided for subsequent measurements. Figure 4 shows the prior austenite grain sizes as a function of reheating temperatures. Error bars represent the standard deviation in PAGS determined form different micrographs.

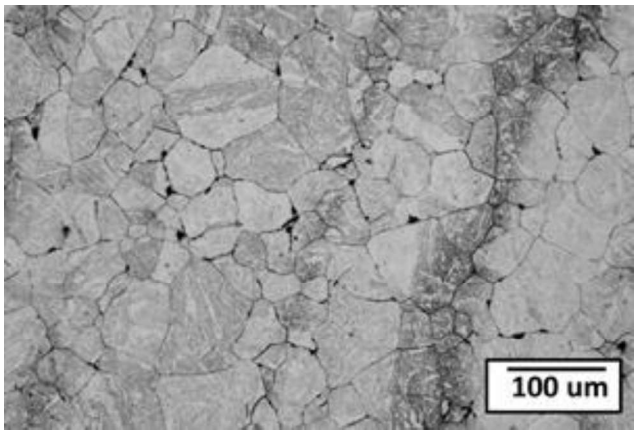

Figure 3: Light micrograph of RH1000 sample, etched with saturated picric acid.

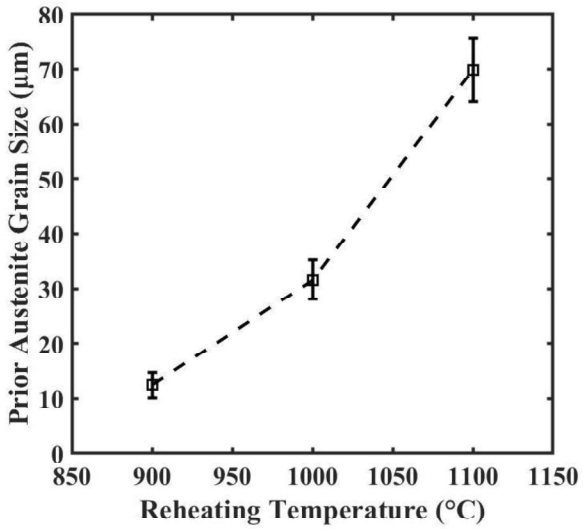

Figure 4: Prior austenite grain size as a function of the reheating temperature during thermal cycling (isothermal holding of 100 s).

Reheating to higher temperatures leads to coarser PAGS. During reheat treatments, austenite reversion takes place, where austenite grains nucleate and grow on PAGBs and at martensite/austenite interfaces. They subsequently impinge against one another resulting in fine austenitic grains and hence fine quenched microstructure. However, during isothermal holding at elevated temperatures, grain growth simultaneously occurs. Larger grains grow at the expense of smaller grains to reduce the grain boundary area of the microstructures.

Grain growth kinetics play an important role in the final PAGS. For an austenite reversion cycle of 1 s at 900 °C, a significantly smaller final PAGS of 5.89 μm ± 0.48 μm was obtained, less than half the value for a 100s hold at 900 °C (RH900). At low reheating temperatures, presence of undissolved cementite or alloy carbides can potentially influence the PAGS. Subsequent thermal cycling at 900 °C did not alter the average grain sizes; however, it was observed that for multiple re-heat cycles, the grain size distribution became narrower. Figure 5 shows the cumulative distribution function (CDF) of grain boundary intercept length for microstructures produced by multiple re-heating cycles (900 °C and 1 s). The triple re-heated sample has a steeper curve as compared to the single re-heated sample, indicating a lower standard deviation in grain size in the triple reheated specimen. Roughly 20 pct of the lineal intercepts in RHS-1 are greater than 10 μm in length while in RHS-3 less than 10 pct intercepts are greater than 10 μm. Lineal intercepts as large as 24.8 μm were observed for RHS-1 sample. Crack nucleation during fatigue in carburized components can occur via inter-granular fracture along PAGBs. Thus larger grains can served as more detrimental nucleation sites and may act as the weak link controlling fatigue performance. The difference in CDF between re-heat conditions indicates that there are fewer large grains after subsequent thermal cycles at elevated temperatures. Thus, owing to a narrower grain size distribution for multiple reheating cycle heat treatments, improved fatigue lives can be expected.

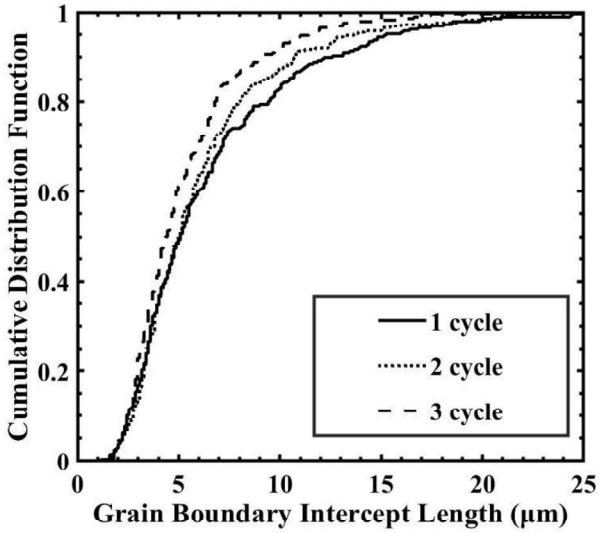

Figure 5: Cumulative distribution function plots for grain boundary linear intercepts of microstructures produced by thermal cycling (900 °C and 1 s) subjected to multiple austenite reversion cycles.

Martensite Micro-Geometry

Figure 6 shows a representative electron micrograph from the RH1000 microstructure etched with 2 pct nital. The dark regions correspond to martensite whereas the light regions are RA. A clear plate morphology of high-carbon martensite can be seen with varying sizes of martensite plates and RA encapsulated in between. Different micro-constituents namely plate martensite (α') and retained austenite (γ) are labeled. Midribs of some martensitic plates are indicated using white lines. The stereological features namely S_V^{MID} and L_V^{MID} (measured in terms of midplane periphery points per unit area, indicated by black circles) are also schematically highlighted.

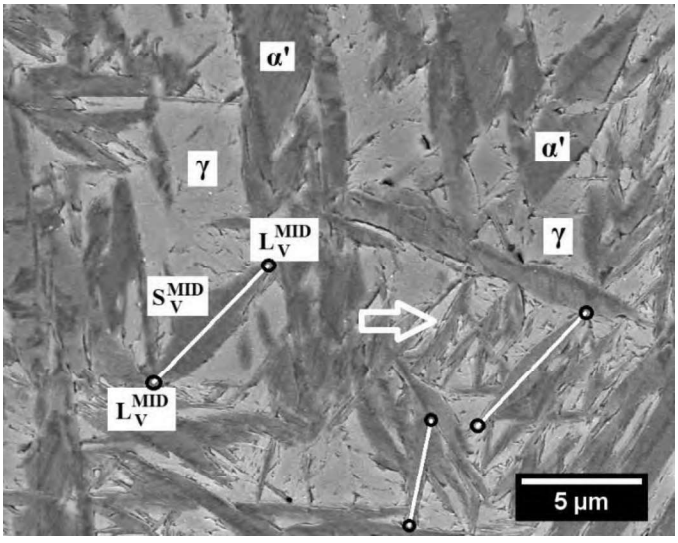

Figure 6: Scanning electron micrograph of a reheat-quenched plate martensite and retained-austenite microstructure etched with 2 pct nital. Constituents and stereological quantities are schematically labeled in the micrograph.

Chen and Winchell have proposed a correlation between shape independent stereological features and the morphological aspects of plate martensite. In this study, two parameters were studied: t_{avg} and r_{avg} [9].

$$t_{avg} = V_V / S_V^{MID}, \text{ and}$$
$$r_{avg} = 2S_V^{MID} / L_V^{MID}$$

The t_{avg} is the average thickness of martensite plate weighted by midplane surface area (S_V^{MID}), r_{avg} is the average distance between center of the plate and its periphery along the midplane, and V_V is the volume fraction of martensite (see figure 2). Hereby, r_{avg} will be referred to as the average martensite plate radius. The stereological results are summarized in Table 2.

Table 2. Summary of Stereological Measurements

Experimental Quantities			
Reheat Temp. (°C)	900	1000	1100
PAGS (µm)	12.4±2.2	31.6±3.6	69.8±5.8
Stereological Quantities			
V_V	0.72±0.01	0.68±0.03	0.72±0.03
S_V^{MID} (µm^{-1})	1.21±0.06	0.86±0.06	0.71±0.04
L_V^{MID}(µm^{-2})	1.1±0.1	0.59±0.05	0.41±0.02
Morphological Quantities			
t_{avg} (µm)	0.59±0.06	0.79±0.07	1.01±0.07
r_{avg} (µm)	2.2±0.24	2.92±0.32	3.46±0.25

All three conditions contain approximately 70 pct martensite by volume and thus a similar degree of austenite partitioning can be assumed. Therefore, it is reasonable to quantitatively compare the micro-geometry of plate martensite for different re-heating treatments. Figure 7 (a) and (b) show the trends in average martensite plate thickness and radius as a function of PAGS where the error bars represent the standard deviation in values obtained from different micrographs. In a given microstructure, a wide range of sizes of martensite plates can be observed. Martensite transformation in the "fill-in" mode initiates with uniform formation of martensite plate in all austenite grains, while the subsequent smaller plates form in the smaller austenite volumes partitioned by previously formed plates, resulting in relatively large values of the reported standard deviations. The white arrow in the micrograph points towards fine martensite plates that potentially partitioned a large RA constituent during fill-in transformation. The mean radius of martensite midrib decreases with an increase in number of units per grain as the transformation progresses [14].

The trends in figure 7 (a) show that the average plate radius decreases with a decrease in PAGS. Guimarães *et al.* [11] suggest that martensite formation proceeds with elastic spread of the midrib followed by thickening of plates. PAGBs and martensite-austenite interfaces are obstacles to the propagation of midribs. The average plate radius is geometrically limited by impingement against physical barriers [11]. Furthermore, as the midrib lengthens, the deformation of austenite in the vicinity of the propagating front impedes its growth, limiting the length of plates [11]. The proposed mechanism is consistent with the trends observed in figure 7(a).

The trends in average plate thickness suggest greater thickness values at higher values of PAGS. As the martensite plate thickens, it deforms the surrounding austenite plastically. Thus, the surrounding austenite imposes a local mechanical constraint over the thickness of plates [11]. The complex interplay of mechanical and geometrical constraints during martensite growth via thickening can potentially explain the trend observed in Figure 7 (b). Previous studies on martensitic transformations in high-carbon steels have shown that t_{avg} is composition dependent [14]. Further, Chang *et al.* [9] reported that the values of t_{avg} are more sensitive to austenite grain size in O1 tool steel than in a Fe-1.4C-0.02P alloy. Chang *et al.* [15] reported t_{avg} and r_{avg} values close to 1 µm and 2 µm for a Fe-1.4C-0.02P alloy, which compare favorably with the values obtained in this investigation. Thus, the growth of martensite and its morphology is limited by both characteristics of the austenite and grain/phase boundary interfaces.

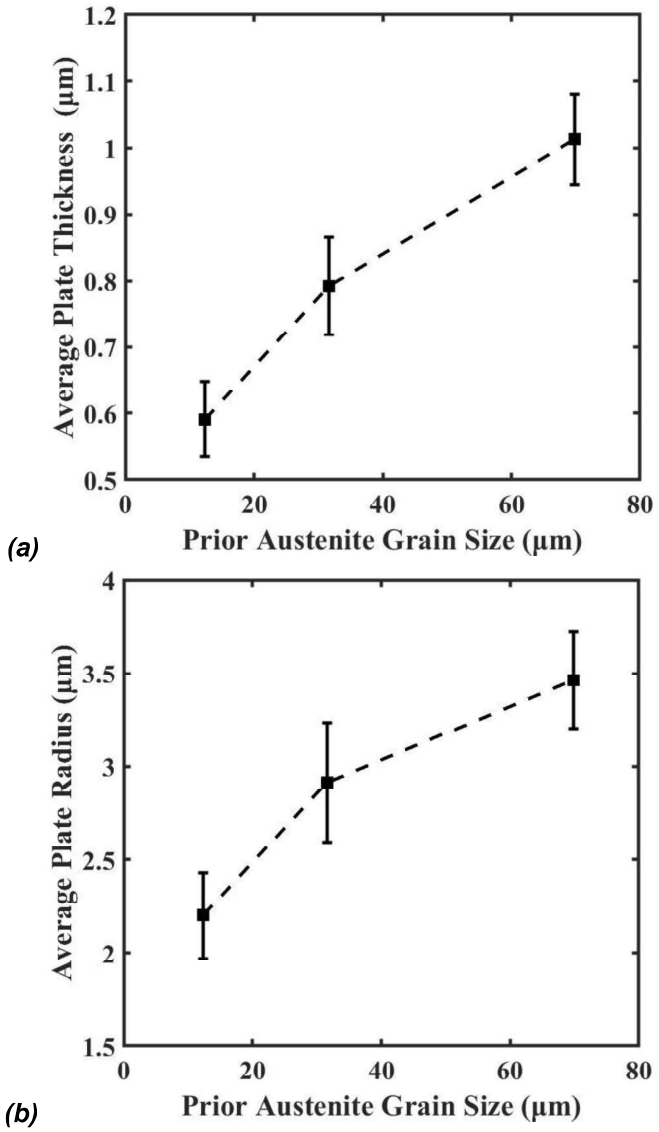

Figure 7: Quantitative trends in morphology of plate martensite as a function of prior austenite grain size of reheated specimen: (a) Average plate thickness and (b) average plate radius.

Retained Austenite Size Distribution

Figure 6 shows a high-carbon martensitic microstructure with RA constituents entrapped between plates of martensite. Austenite grain partitions as the transformation progresses and a wide range of constituent sizes are obtained. Using thresholding in MIPAR, an image processing software, areas of disconnected austenitic regions were identified in 2-D planes and their circular equivalent diameters were determined. The size distribution of the RA constituents per unit area was determined, given by $(N_A)_i$, the number of RA constituents in each class interval, i, with diameter D_i. The average RA constituent diameter, D_{avg} is given by

$$D_{avg} = \frac{1}{N_V}\left(\sum (N_V)_i D_i\right)$$

where $(N_V)_i$ is the number of constituents per unit volume in each class interval. N_V is not a measurable quantity in micrographs, however, it can be correlated to N_A by considering the probability of the test plane sectioning the RA constituents.

The Schwartz-Saltykov method was employed to determine the RA constituent size distribution $(N_V)_i$ [13]. The method was originally proposed for poly-dispersed system of spheres, with inaccuracies resulting from non-spherical shapes. However, reasonable trends can be determined for equiaxed and spheroidal particles, with such a simple analysis [13]. Figure 8 shows the trend in average RA constituent diameter as a function of PAGS. Figure 9 (a), (b) and (c) shows the frequency distribution curves for RA constituent sizes in RH900, RH1000 and RH1100 microstructures, respectively.

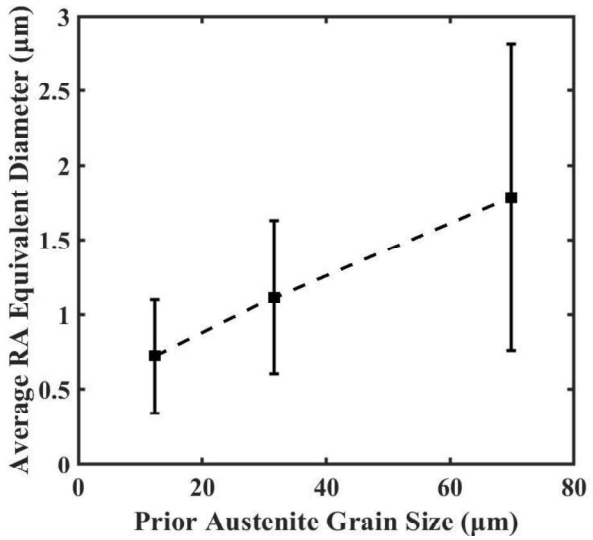

Figure 8: Average equivalent diameter of the RA constituents as a function of prior austenite grain size (PAGS) of reheated specimen.

The average RA constituent diameter increases with an increase in prior austenite grain size of the microstructure. Since all the conditions have approximately the same volume fraction of RA, the influence PAGS can be isolated in these conditions. The linear trend for average RA diameter can thus be primarily attributed to geometrically constrained spread of martensite in different PAGS. RA constituents share interfaces with plate martensite. As discussed in the previous section, finer PAGS results in finer martensite plates, and thus a greater surface area to volume ratio (S_V^{MID}). Therefore, finer RA constituents are found in fine PAGS microstructures.

It can also be observed in figure 8 that the standard deviation in RA diameter increases with increase in PAGS, suggesting that a larger range of RA constituent sizes are present in RH1100 as compared to RH900. The frequency distribution plots in figure 9 show the same trends.

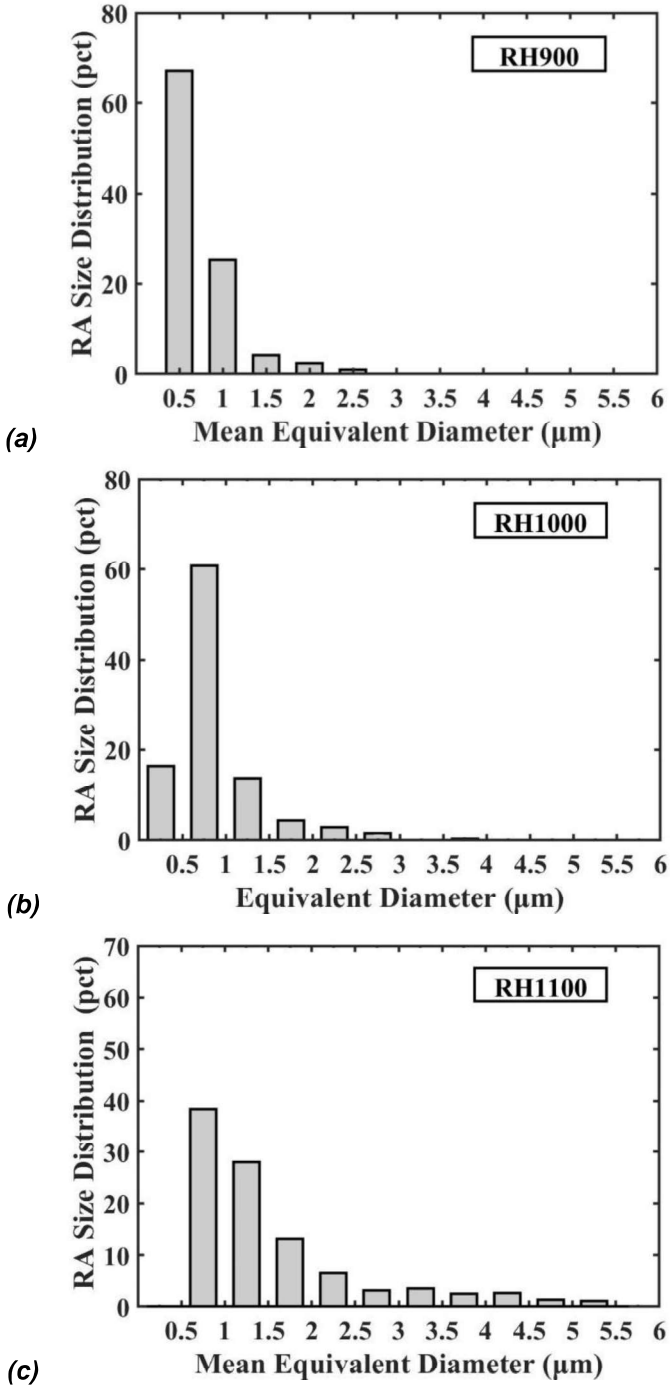

Figure 9: Size distribution of RA constituents in reheated specimen: (a) RH900, (b)RH1000 and (c)RH1100. The number fraction of constituents is plotted against equivalent diameter.

The span of the distribution and the size of largest austenite constituent increases with increase in PAGS. In the existing literature pertaining to RA containing advanced-high-strength-sheet (AHSS) steels, the stability of RA has been attributed to factors such as composition, size, shape and strain partitioning in surrounding microstructures [16–18]. Even though the sub-micron constituents form the greatest fraction of RA, they are potentially mechanically stable at low stresses. The size distribution data suggests that constituents with diameter greater than 2.5 μm contribute to approximately 75 pct RA by volume in RH1100, and approximately 25 pct RA by volume in RH1000, while all the RA constituents in RH900 are finer than 2.5 μm.

It is hypothesized that microstructural refinement from thermal cycling resulting in a fine distribution of RA constituents can consequently affect the mechanical behavior, e.g. fatigue.

Conclusions

Microstructure development during thermal cycling of commercial high-carbon 52100 steel was investigated.

- The thermal cycling heat treatment is an effective approach for PAGS control. During reheating above the A_3 temperature, low temperatures and short isothermal holdings resulted in the greatest grain size refinement.
- Multiple reheating cycles did not substantially reduce the PAGS further. However, a narrower PAGS distribution was obtained, potentially resulting in a reduced number of large intergranular crack nucleation sites in fatigue.
- The average martensite plate radius and plate thickness increase with increase in PAGS. The growth of martensite and its morphology are limited by physical obstacles such as grain/phase boundary interfaces.
- Stereological measurements on plate martensite and RA constituents showed that finer PAGS leads to finer plates and RA constituents. Since the mechanical stability of austenite depends on its size, grain refinement can potentially lead to a more stable retained austenite in carburized components.

Acknowledgments

This research project is being supported by NSF-CMMI award number 1728007. The authors also gratefully acknowledge the support of the sponsors of Advanced Steel Processing and Products Research Center at Colorado School of Mines, especially TimkenSteel, for providing the raw material for this investigation.

References

[1] H. Mohrbacher, "Metallurgical concepts for optimized processing and properties of carburizing steel," *Advances in Manufacturing*, vol. 4, (2016). doi:10.1007/s40436-016-0142-9.

[2] G. Krauss, "Fatigue and Fracture," in *ASM Handbook.Vol.19*, ASM International, pp. 680–690, (1996). doi:10.31399/asm.hb.v19.9781627081931.

[3] J. P. Wise and D. K. Matlock, "Bending Fatigue of Carburized Steels: A Statistical Analysis of Process and Microstructural Parameters," SAE Transactions, vol. 109, pp. 182-191, (2000). doi:10.4271/2000-01-0611.

[4] C. A. Apple and G. Krauss, "Microcracking and fatigue in a carburized steel," *Metallurgical Transactions*, vol. 4, no. 5, pp. 1195–1200, (May 1973). doi:10.1007/BF02644511.

[5] S. M. C. Van Bohemen and J. Sietsma, "Martensite Formation in Partially and Fully Austenitic Plain Carbon Steels," *Metallurgical and Materials Transactions A*, vol. 40, no. 5, pp. 1059–1068, (May 2009). doi:10.1007/s11661-009-9796-2.

[6] S. M. C. van Bohemen and J. Sietsma, "Kinetics of martensite formation in plain carbon steels: critical assessment of possible influence of austenite grain boundaries and autocatalysis," *Materials Science and Technology*, vol. 30, no. 9, pp. 1024–1033, (Jul. 2014). doi:10.1179/1743284714Y.0000000532.

[7] A. R. Entwisle, "The kinetics of martensite formation in steel," *Metallurgical Transactions*, vol. 2, no. 9, pp. 2395–2407, (Sep. 1971). doi:10.1007/BF02814877.

[8] C. H. Shih, B. L. Averbach, and M. Cohen, "Some Characteristics of the Isothermal Martensitic Transformation," *JOM*, vol. 7, no. 1, pp. 183–187, (Jan. 1955). doi:10.1007/BF03377476.

[9] P. H. Chang, P. G. Winchell, and G. L. Liedl, "Quantitative geometric characterization of high carbon martensite," *Metallurgical Transactions A*, vol. 14, no. 1, pp. 163–173, (Feb. 1983). doi:10.1007/BF02651612.

[10] P. R. Rios and J. R. C. Guimarães, "Microstructural path analysis of athermal martensite," *Scripta Materialia*, vol. 57, no. 12, pp. 1105–1108, (Dec. 2007). doi:10.1016/J.SCRIPTAMAT.2007.08.019.

[11] J. R. C. Guimarães and P. R. Rios, "Spatial Aspects of Martensite," *Metallurgical and Materials Transactions A*, vol. 43, no. 7, pp. 2218–2224, (Jul. 2012). doi:10.1007/s11661-012-1102-z.

[12] J. R. C. Guimarães and J. C. Gomes, "A metallographic study of the influence of the austenite grain size on martensite kinetics," *Acta Metallurgica*, vol. 26, no. 10, pp. 1591–1596, (Oct. 1978). doi:10.1016/0001-6160(78)90068-8.

[13] E. E. Underwood, "Quantitative Stereology for Microstructural Analysis," in *Microstructural Analysis*, Boston, MA: Springer US, pp. 35–66, (1973). doi:10.1007/978-1-4615-8693-7_3.

[14] J. R. C. Guimarães, “Athermal martensite: Genesis of microstructure and transformation curves,” *Materials Science and Engineering: A*, vol. 476, no. 1–2, pp. 106–111, (Mar. 2008). doi:10.1016/J.MSEA.2007.04.068.

[15] P. H. Chang, H. Rubin, P. G. Winchell, and G. L. Liedl, “The determination of size distribution of martensite plates by Kernel estimation,” *Scripta Metallurgica*, vol. 16, no. 5, pp. 531–536, (May 1982). doi:10.1016/0036-9748(82)90264-2.

[16] I. B. Timokhina, P. D. Hodgson, and E. V. Pereloma, “Effect of microstructure on the stability of retained austenite in transformation-induced-plasticity steels,” *Metallurgical and Materials Transactions A*, vol. 35, no. 8, pp. 2331–2341, (Aug. 2004). doi:10.1007/s11661-006-0213-9.

[17] J. H. Ryu, D.-I. Kim, H. S. Kim, H. K. D. H. Bhadeshia, and D.-W. Suh, “Strain partitioning and mechanical stability of retained austenite,” *Scripta Materialia*, vol. 63, no. 3, pp. 297–299, (Aug. 2010). doi: 10.1016/J.SCRIPTAMAT.2010.04.020.

[18] S. Zhang and K. O. Findley, “Quantitative assessment of the effects of microstructure on the stability of retained austenite in TRIP steels,” *Acta Materialia*, vol. 61, no. 6, pp. 1895–1903, (Apr. 2013). doi: 10.1016/j.actamat.2012.12.010